Experimental demonstration of a broadband TM-pass polarizer based on tilted subwavelength metamaterials

Miguel Barona-Ruiz[(1),*], Carlos Pérez-Armenta[(1)], Alejandro Ortega-Moñux[(1)],
J. Gonzalo Wangüemert-Pérez[(1)], Íñigo Molina-Fernández[(1)], Pavel Cheben[(2)] and Robert Halir[(1)]
[*]miguelbr@uma.es
[(1)]Telecommunication Research Institute (TELMA), Universidad de Málaga, Louis Pasteur 35, 29010 Málaga, Spain.
[(2)]National Research Council Canada, Ottawa, Ontario K1A 0R6, Canada.

***Abstract*—On-chip polarizers have been used extensively to control the polarization of integrated photonic systems based on the Silicon-On-Insulator platform, which present a strong birrefringence. Designing polarizers that attenuate TE polarized light while permitting TM polarized light to pass with minimal losses presents notable challenges on the standard 220 nm Silicon-on-Insulator platform due to the stronger confinement experienced by TE polarization compared to TM polarization. In this work, we present and experimentally demonstrate a broadband, low-loss, high-extinction-ratio TM-pass polarizer utilizing a Bragg grating. By leveraging a subwavelength metamaterial, we manipulate the Bragg grating to reflect the fundamental TE mode into the first-order TE mode while enabling the transmission of the TM mode. Experimental results show an extinction ratio exceeding 20 dB and insertion losses below 1 dB within a bandwidth of at least 120 nm.**

I. Introduction

Silicon-on-Insulator (SOI) is increasingly becoming the platform of choice to implement integrated photonic systems for telecom, datacom, sensing and computing [1]. The high index contrast of this platform enables strong mode confinement but also induces significant birrefringence between TE and TM polarizations. Therefore, polarization control is key in SOI-based photonic systems. One of the main devices used to manage polarization are polarizers, which block the unwanted polarization and let the remaining one pass through it with no losses. In standard SOI platforms, TE polarization is more confined than TM polarization. This results in TM-pass polarizers requiring more complex designs than TE-pass polarizers. Nonetheless, they are essential components in applications based on TM-polarization like biosensing, since the TM polarization is less confined and has a stronger interaction with the sensed media [2]; and high-speed optical communications, where polarization-division-multiplexing (PDM) is widely used.

Some TM-pass polarizer designs take advantage of specialized silicon layer thicknesses such as $300\,\mathrm{nm}$, $340\,\mathrm{nm}$ and $400\,\mathrm{nm}$ to cut-off the fundamental TE mode, since the TM fundamental mode is more confined [3]–[5]. On the other hand, in the standard $220\,\mathrm{nm}$ thickness, TE-pass polarizers leverage the weaker confinement of the TM modes while the TE mode remains guided [6]–[8]. For this reason, implementing TM-pass polarizers in this thickness proves challenging, and complex waveguide structures such as graphene-loaded waveguides [9], [10], multilayer structures [11], or plasmonic waveguides [12]–[15] have been presented. Another approach is to use Bragg gratings [16]–[24]. However, they reflect the TE fundamental mode back into the system, which can be potentially harmful for certain applications.

Several solutions to this problem have been experimentally demonstrated. In [25], a Bragg grating with narrow slots that radiates the TE polarization with a bandwidth of more than $95\,\mathrm{nm}$, insertion losses (IL) as low as $0.5\,\mathrm{dB}$ and a extinction ratio (ER) as high as $50\,\mathrm{dB}$; however the narrow designed $50\,\mathrm{nm}$ slots can prove difficult to fabricate. An apodized anti-symmetric Bragg grating that reflects the fundamental TE mode into the first order TE mode and filters it is demonstrated in [26], achieving a bandwidth of $263\,\mathrm{nm}$ with IL lower than $0.9\,\mathrm{dB}$ and a maximum ER of $50\,\mathrm{dB}$; nevertheless, it is designed with holes as small as $50\,\mathrm{nm}$, which again is challenging to fabricate. A tapered anti-symmetric Bragg grating that works in two bands is designed and measured, obtaining an IL smaller than $0.74\,\mathrm{dB}$ and an ER as great as $60\,\mathrm{dB}$, over a bandwidth of $85\,\mathrm{nm}$ for the O-band and $35\,\mathrm{nm}$ for the S-band is reported in [27].

In this paper, we present and experimentally demonstrate a TM-pass polarizer for the standard $220\,\mathrm{nm}$ SOI platform fabricated with a single etch-step. By taking advantage of the flexibility of subwavelength metamaterials we design a Bragg grating that reflects the fundamental TE mode into the first order TE mode while letting the fundamental TM mode pass with no losses. The back-reflected first order mode is radiated, thereby suppressing back-reflections. The fabricated device achieves a measured extinction ratio in excess of $20\,\mathrm{dB}$, insertion losses below $1\,\mathrm{dB}$ in a bandwidth of at least $120\,\mathrm{nm}$.

II. Polarizer structure and design

The polarizer consists of a periodic structure, shown in the unit cell in Fig. 1(a). If the tilt angle is $\theta = 0°$ [Fig. 1(b)] the unit cell operates in the subwavelength regime, i.e. the pitch is such that $\Lambda_{\mathrm{SWG}} < \lambda/(2n_{\mathrm{B}})$, where n_B is the effective index of the fundamental Bloch-Floquet mode propagating through the structure [28]. In this regime light propagates through the structure undisturbed for both TE and TM polarization. However, when the second strip strip is tilted an angle $\theta \neq 0$ the period of the structure becomes $\Lambda_{\mathrm{Bragg}} = 2\Lambda_{\mathrm{SWG}}$ [see Fig. 1(b-d)]. This tilt only affects TE modes [29], which thus experience a Bragg reflection. TM modes are unaffected by the tilt, and travel through the structure as they would in a

conventional subwavelength grating (SWG). This differential behaviour for TE/TM polarization gives rise to the desired polarizing effect.

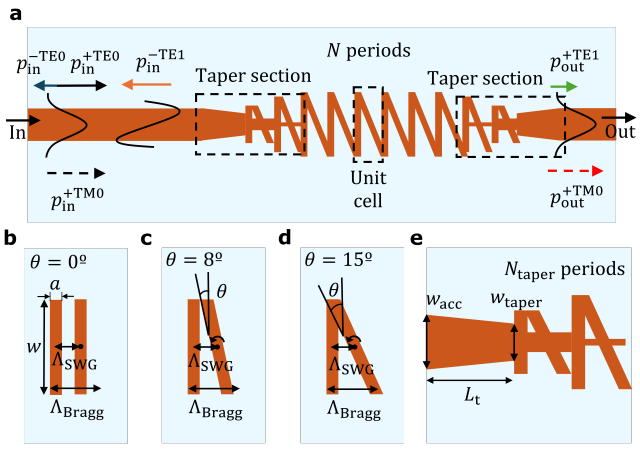

Fig. 1. Schematics of the proposed device. (a) Top view of the complete device: the TM_0 mode goes through it with low losses, while the TE_0 mode gets reflected into the TE_1 mode. (b), (c) and (d) Top diagram of the unit-cell of the device, tilted $\theta = 0°$, $\theta = 8°$ and $\theta = 15°$, respectively. (e) Schematic top-view of the polarizer's taper.

For the device to couple the TE_0 forwards propagating mode into the TE_1 backward propagating mode which can be easily radiated, the phase matching condition between said modes must be met: $n_{\mathrm{B},0} + n_{\mathrm{B},1} = \lambda/\Lambda_{\mathrm{Bragg}}$ [30]. Thus, we can satisfy the phase matching condition by carefully engineering the Bragg pitch Λ_{Bragg}. We note that the lower and upper values for Λ_{Bragg}, are limited by the minimum feature size and the SWG condition of the period Λ_{SWG}, respectively. We use the MPB software package [31] to calculate the pitch that centers the phase-matching condition at a wavelength of $\lambda = 1.55\,\mu\mathrm{m}$, obtaining $\Lambda_{\mathrm{Bragg}} = 440\,\mathrm{nm}$.

There are four figures of merit to measure the performance of a polarizer. To define them we use the notation $p_{\mathrm{in/out}}^{\pm \mathrm{TE/TM}n}$ to refer to the power travelling in the forward (+) or backward (-) direction, in the nth-order mode in TE/TM polarization in the input (in) or output (out) port. Thus, the key performace parameters of a polarizer are: the extinction ratio: $\mathrm{ER} = p_{\mathrm{out}}^{+\mathrm{TM0}}/p_{\mathrm{out}}^{+\mathrm{TE0}}$; the insertion losses: $\mathrm{IL} = p_{\mathrm{out}}^{+\mathrm{TM0}}/p_{\mathrm{in}}^{+\mathrm{TM0}}$; the undesired back-reflections to the fundamental TE mode: $\mathrm{BR0} = p_{\mathrm{in}}^{-\mathrm{TE0}}/p_{\mathrm{in}}^{+\mathrm{TE0}}$; and the back-reflections to the first order TE mode: $\mathrm{BR1} = p_{\mathrm{in}}^{-\mathrm{TE1}}/p_{\mathrm{in}}^{+\mathrm{TE0}}$. We want to maximize the extinction ratio (ER) and the back-reflections to the first order TE mode (BR1) while minimizing the insertion losses (IL) and the back-reflections to the fundamental TE mode (BR0), over the broadest bandwidth possible. We optimize this parameters using MEEP [32], a 3D-FDTD open source simulator, arriving at the final design: $\Lambda_{\mathrm{Bragg}} = 440\,\mathrm{nm}$, $\theta = 15°$, $w = 1.1\,\mu\mathrm{m}$, $a = 110\,\mathrm{nm}$, $N = 20$ periods. However, insertion losses were still excessively high ($> 1\,\mathrm{dB}$), so a taper was designed to minimize them, shown in Fig. 1 (e), with the following parameters: $L_{\mathrm{taper}} = 500\,\mathrm{nm}$, $w_{\mathrm{acc}} = 500\,\mathrm{nm}$, $w_{\mathrm{taper}} = 300\,\mathrm{nm}$, $N_{\mathrm{taper}} = 8$ periods.

The simulated polarizer propagation of both TE and TM fundamental modes at the central wavelength $\lambda = 1.55\,\mu\mathrm{m}$ can be observed at Fig. 2 (a) and (b), respectively, where it is clear how the TE fundamental mode gets reflected into the TE first order mode while the TM mode traverses the polarizer with almost no losses. Then, the polarizer's performance is simulated varying the operating wavelength from $1.45\,\mu\mathrm{m}$ to $1.65\,\mu\mathrm{m}$, shown in Fig. 3. From the figure we can see that for a $150\,\mathrm{nm}$ bandwidth around the central wavelength of $1.55\,\mu\mathrm{m}$, the extinction ratio is greater than $20\,\mathrm{dB}$ while the insertion losses are below $1\,\mathrm{dB}$. Moreover, the harmful back-reflections of the fundamental TE mode are kept below $-20\,\mathrm{dB}$ for most of the $150\,\mathrm{nm}$ bandwidth whereas the back reflections into the first order TE mode are maximized.

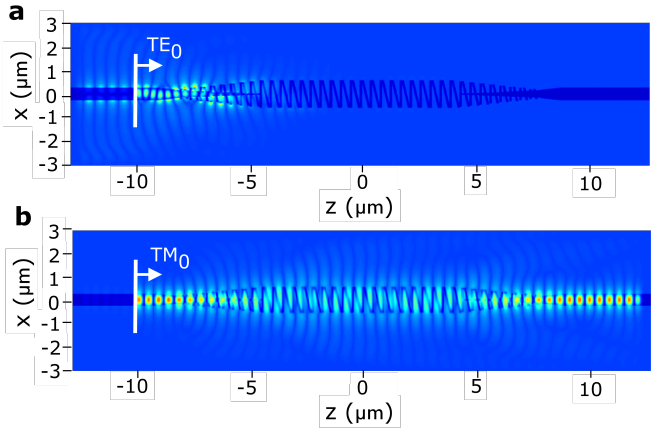

Fig. 2. Propagation of (a) the TE_0 and (b) the TM_0 modes along the designed device at a working wavelength of $1.55\,\mu\mathrm{m}$. As intended, the TE_0 mode gets reflected into the TE_1 mode, while the TM_0 mode traverses the polarizer with minimal losses.

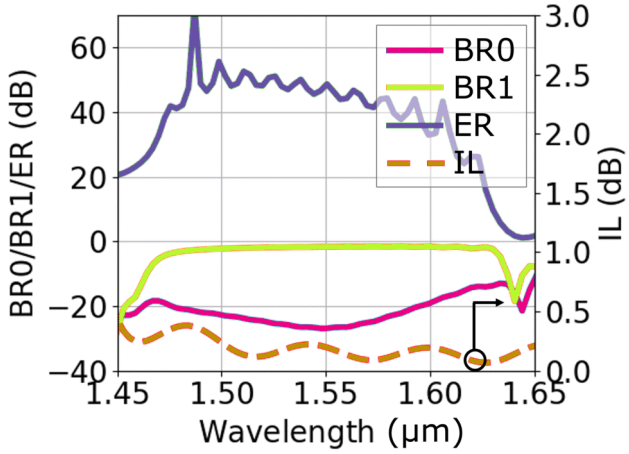

Fig. 3. Simulated key parameters of the polarizer as a function of the wavelength. The dashed red line, corresponding to the IL, is referenced on the right axis, while the rest of the curves are referenced to the left axis.

III. Experimental Characterization

The proposed device is then fabricated in a $220\,\mathrm{nm}$-thick SOI platform, with a buried oxide layer of $2\,\mu\mathrm{m}$ thickness, using Applied Nanotool's standard process [33]. Resist is patterned with a $100\,\mathrm{keV}$ electron-beam, and structures are transferred into the silicon layer via reactive ion etching. A $2.2\,\mu\mathrm{m}$-thick oxide layer is placed on the top using chemical vapour deposition. SEM images of the complete polarizer, the first periods of the taper and a detailed view of the central

periods can be observed in Figs. 4 (a), (b) and (c), respectively. The device is measured using the Agilent 8164B lightwave measurement system, equipped with a 81600B tunable laser output and a 81634B power sensor. Following the laser output, two external polarization controllers, with a polarization filter placed in between them, are used. With this approach, we can filter any spurious polarization at the laser output thanks to the polarization filter and the first polarization controller. Then, with the second polarization controller, we can set the desired polarization at the chip input. To inject the light in and out the chip, we use two lensed fibers, along with on-chip input and output spot size converters to improve the coupling between the lensed fibers and the on-chip waveguides. A test structure consisting of the designed polarizer with nominal parameters, except for a increased strip length of $a = 130\,\mathrm{nm}$, is measured with TE and TM polarization, sweeping the wavelength along the laser's tunable bandwidth: $1495\,\mathrm{nm} - 1640\,\mathrm{nm}$. After this, a straight waveguide is measured as reference for both polarizations. The performance parameters are obtained from the test structure measurements and then normalized to the power measured at the straight waveguides for each polarization. Then, the measured parameters are compared with the simulated results and represented in Fig. 5. As can be seen, the measured ER response is shifted to longer wavelengths with respect to the simulated ER due to the increased strip length. The difference of $20\,\mathrm{dB}$ between the simulated and measured ER should be noted as well. This seeming great difference is caused by the difficulty involved in using the polarization controller preceding the chip input to filter the power of the TM polarization below $0.1\,\%$ ($30\,\mathrm{dB}$) and measure the actual ER of the polarizer. The measured IL, on the other hand, grows as it approaches the limit of its operational bandwidth. The measurements taken show that for a bandwidth of at least $120\,\mathrm{nm}$, the polarizer has an ER larger than $20\,\mathrm{dB}$ while it keeps the IL under $1\,\mathrm{dB}$.

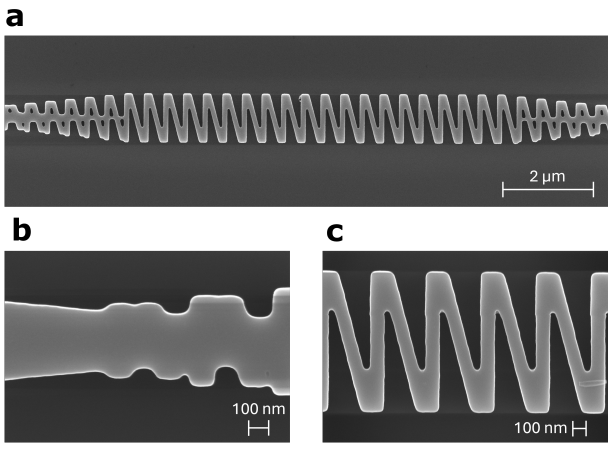

Fig. 4. SEM images of the a) complete device, b) the first two periods of the transition and c) five central periods of the polarizer.

IV. Conclusions

In this work, we have proposed and experimentally demonstrated for the first time a design for a compact TM-pass polarizer based on a tilted SWG for the standard $220\,\mathrm{nm}$-thick SOI platform and fabricated with a single etch-step. The tilted

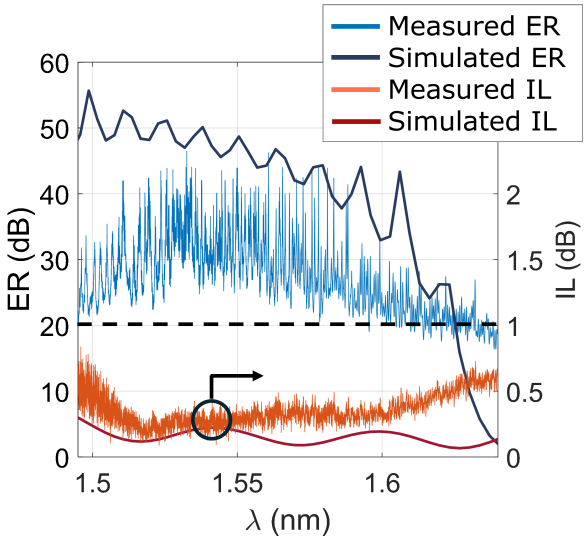

Fig. 5. Comparison between the measured and simulated ER (left axis) and IL (right axis) spectra.

SWG enables the coupling between the undesired fundamental TE mode into the reflected first order TE mode, which can be readily removed. On the other hand, the TM fundamental mode pass through the polarizer with low losses. Experimental characterization shows that the polarizer presents low insertion losses ($< 1\,\mathrm{dB}$) and a high extinction ratio ($> 20\,\mathrm{dB}$) over more than a $120\,\mathrm{nm}$ bandwidth, centered at a wavelength of $1.55\,\mu\mathrm{m}$. Altogether, the fabricated polarizer has total footprint of $17.84\,\mu\mathrm{m} \times 1.1\,\mu\mathrm{m}$.

Acknowledgements

This work has received funding from the Ministerio de Universidades, Ciencia e Innovacion under project PID2022-139540OB-I00 and project TED2021-130400B-I00/ AEI/10.13039/501100011033/ Unión Europea NextGenerationEU/PRTR.

References

[1] S. Shekhar, W. Bogaerts, L. Chrostowski, J. E. Bowers, M. Hochberg, R. Soref, and B. J. Shastri, "Roadmapping the next generation of silicon photonics," *Nature Communications*, vol. 15, no. 1, p. 751, 2024.

[2] S. Tanev, A. Densmore, D.-X. Xu, S. Janz, P. Waldron, J. Lapointe, T. Mischki, G. Lopinski, A. Delâge, J. H. Schmid, and P. Cheben, "Sensitive label-free biomolecular detection using thin silicon waveguides," *Advances in Optical Technologies*, vol. 2008, p. 725967, 2008.

[3] S. I. H. Azzam, M. F. O. Hameed, N. F. F. Areed, M. M. Abd-Elrazzak, H. A. El-Mikaty, and S. S. A. Obayya, "Proposal of an ultracompact CMOS-compatible TE-/TM-pass polarizer based on SOI platform," *IEEE Photonics Technology Letters*, vol. 26, no. 16, pp. 1633–1636, 2014.

[4] W. Liu, S. Zhao, H. Li, D. Dai, and Y. Shi, "Ultra-high performance all-silicon tm polarizer covering o-u optical communication bands," *Journal of Lightwave Technology*, vol. 40, no. 22, pp. 7326–7332, 2022.

[5] Q. Wang and S.-T. Ho, "Ultracompact TM-pass silicon nanophotonic waveguide polarizer and design," *IEEE Photonics J.*, vol. 2, no. 1, pp. 49–56, 2010.

[6] Y. Xiong, D.-X. Xu, J. H. Schmid, P. Cheben, and W. N. Ye, "High extinction ratio and broadband silicon TE-pass polarizer using subwavelength grating index engineering," *IEEE Photonics J.*, vol. 7, no. 5, pp. 1–7, 2015.

[7] H. Zafar, P. Moreira, A. M. Taha, B. Paredes, M. S. Dahlem, and A. Khilo, "Compact silicon TE-pass polarizer using adiabatically-bent fully-etched waveguides," *Opt. Express*, vol. 26, pp. 31850–31860, Nov 2018.

[8] D. Dai, Z. Wang, N. Julian, and J. E. Bowers, "Compact broadband polarizer based on shallowly-etched silicon-on-insulator ridge optical waveguides," *Opt. Express*, vol. 18, pp. 27404–27415, Dec 2010.

[9] X. Hu and J. Wang, "Ultrabroadband compact graphene–silicon TM-pass polarizer," *IEEE Photonics J.*, vol. 9, no. 2, pp. 1–10, 2017.

[10] W. S. Chong, S. X. Gan, C. K. Lai, W. Y. Chong, D. Choi, S. Madden, R. M. De La Rue, and H. Ahmad, "Configurable TE- and TM-pass graphene oxide-coated waveguide polarizer," *IEEE Photonics Technol. Lett.*, vol. 32, no. 11, pp. 627–630, 2020.

[11] S. I. Azzam and S. S. A. Obayya, "Ultra-compact resonant tunneling-based TE-pass and TM-pass polarizers for SOI platform," *Opt. Lett.*, vol. 40, pp. 1061–1064, Mar 2015.

[12] L. Sánchez, S. Lechago, and P. Sanchis, "Ultra-compact TE and TM pass polarizers based on vanadium dioxide on silicon," *Opt. Lett.*, vol. 40, pp. 1452–1455, Apr 2015.

[13] B. Bai, L. Liu, R. Chen, and Z. Zhou, "Low loss, compact TM-pass polarizer based on hybrid plasmonic grating," *IEEE Photonics Technol. Lett.*, vol. 29, no. 7, pp. 607–610, 2017.

[14] X. Zhang, Y. Li, L. Fan, C. Peng, Y. Wu, M. Zou, W. Zhao, J. Li, J. Zhuang, J. Yan, J. Mei, and X. Wang, "Design and simulation of tunable te and tm pass polarizers based on vo2/si hybrid waveguide," *Optics Communications*, vol. 502, p. 127413, 2022.

[15] X. Yang, J. Xu, T. Chi, T. Zhou, M. Chen, J. Wang, N. Liu, Y. Lu, and Z. Liang, "Compact and low-loss tm-pass polarizer based on a hybrid plasmonic waveguide with a semiround arch si core," *Appl. Opt.*, vol. 61, pp. 6571–6576, Aug 2022.

[16] X. Guan, P. Chen, S. Chen, P. Xu, Y. Shi, and D. Dai, "Low-loss ultracompact transverse-magnetic-pass polarizer with a silicon subwavelength grating waveguide," *Opt. Lett.*, vol. 39, pp. 4514–4517, Aug 2014.

[17] Z. Xu, T. Lyu, and X. Sun, "Interleaved subwavelength gratings strip waveguide based TM pass polarizer on SOI platform," *IEEE Photonics J.*, vol. 12, no. 2, pp. 1–10, 2020.

[18] Y. He, Y. Zhang, R. Zhang, L. Sun, and Y. Su, "Ultra-compact and broadband silicon polarizer employing a nanohole array structure," *Opt. Lett.*, vol. 46, pp. 194–197, Jan 2021.

[19] D. W. Kim, M. H. Lee, Y. Kim, and K. H. Kim, "Ultracompact transverse magnetic mode-pass filter based on one-dimensional photonic crystals with subwavelength structures," *Opt. Express*, vol. 24, pp. 21560–21565, Sep 2016.

[20] W. Zhou, Y. Tong, X. Sun, and H. K. Tsang, "Ultra-broadband hyperuniform disordered silicon photonic polarizers," *IEEE J. Sel. Top. Quantum Electron.*, vol. 26, no. 2, pp. 1–9, 2020.

[21] G. Cheng, Q. Li, Q. Yi, Z. Yan, F. Xu, X. Xiong, Z. Shen, C. Sima, H. Li, and L. Shen, "Multi-band all-silicon tm-pass polarizer based on one-dimensional photonic crystals nanohole array," *Opt. Lett.*, vol. 48, pp. 6072–6075, Nov 2023.

[22] S. Wu, Z. Guo, T. Feng, J. Xiao, and X. S. Yao, "Compact and ultra-broadband all-silicon tm-pass and te-reflected polarizer using grating based weakly coupled nanowires," *Opt. Express*, vol. 30, pp. 29844–29855, Aug 2022.

[23] Y. Yu, Z. Guo, S. Wu, and J. Xiao, "Demonstration of an ultra-compact and broadband tm-pass polarizer using nano-elliptical holes," *IEEE Photonics Technology Letters*, vol. 36, no. 7, pp. 461–464, 2024.

[24] Y. Dong, Y. Liu, Y. Xu, and B. Zhang, "An ultra-broadband design of tm-pass/te-stop polarizer based on multistage bragg gratings," *Photonics*, vol. 9, no. 6, 2022.

[25] H. Zafar, M. Odeh, A. Khilo, and M. S. Dahlem, "Low-loss broadband silicon TM-pass polarizer based on periodically structured waveguides," *IEEE Photonics Technol. Lett.*, vol. 32, no. 17, pp. 1029–1032, 2020.

[26] G. Cheng, Q. Yi, Z. Yan, Q. Li, F. Xu, C. Sima, and L. Shen, "Ultrahigh-extinction-ratio and broadband all-silicon TM-pass polarizer by employing multimode anti-symmetric apodized Bragg grating," *APL Photonics*, vol. 8, p. 046112, 04 2023.

[27] W. Liu, X. Fu, C. Cheng, and L. Yang, "High-performance tm-pass polarizer based on anti-symmetric bragg gratings," *Opt. Express*, vol. 31, pp. 44148–44159, Dec 2023.

[28] J. M. Luque-González, A. Sánchez-Postigo, A. Hadij-ElHouati, A. Ortega-Moñux, J. G. Wangüemert-Pérez, J. H. Schmid, P. Cheben, Íñigo Molina-Fernández, and R. Halir, "A review of silicon subwavelength gratings: building break-through devices with anisotropic metamaterials," *Nanophotonics*, vol. 10, no. 11, pp. 2765–2797, 2021.

[29] J. M. Luque-González, A. Herrero-Bermello, A. Ortega-Moñux, Íñigo Molina-Fernández, A. V. Velasco, P. Cheben, J. H. Schmid, S. Wang, and R. Halir, "Tilted subwavelength gratings: controlling anisotropy in metamaterial nanophotonic waveguides," *Opt. Lett.*, vol. 43, pp. 4691–4694, Oct 2018.

[30] M. Barona-Ruiz, C. Pérez-Armenta, A. Ortega-Moñux, J. G. Wangüemert-Pérez, I. Molina-Fernández, P. Cheben, and R. Halir, "Broadband and low-loss tm-pass polarizer using tilted subwavelength structures," *Opt. Express*, vol. 30, pp. 38930–38937, Oct 2022.

[31] S. G. Johnson and J. D. Joannopoulos, "Block-iterative frequency-domain methods for maxwell's equations in a planewave basis," *Opt. Express*, vol. 8, pp. 173–190, Jan 2001.

[32] A. F. Oskooi, D. Roundy, M. Ibanescu, P. Bermel, J. Joannopoulos, and S. G. Johnson, "Meep: A flexible free-software package for electromagnetic simulations by the fdtd method," *Comput. Phys. Commun.*, vol. 181, no. 3, pp. 687–702, 2010.

[33] "Applied nanotools inc. — x-ray optics and integrated photonics." https://www.appliednt.com/.